工學碩士學位論文

Folic Acid Conjugated Silica-titania Hollow Nanoparticle Targeting MCF-7 Cells for Photodynamic Therapy

엽산수식 실리카-티타니아 중공구조 구형나노입자로 표적화된 MCF-7 세포에 대한 광역동치료

2014年 2月

서울大學校 大學院

化學生物工學部

張 允 宣

↑
2cm
↓

Folic Acid Conjugated Silica-titania Hollow Nanoparticle Targeting MCF-7 Cells for Photodynamic Therapy
2014

2014

張允宣

↑
2.5cm
↓

↑
4cm
↓

↑
3cm
↓

↑
2cm
↓

Folic Acid Conjugated Silica-titania Hollow Nanoparticle Targeting MCF-7 Cells for Photodynamic Therapy

지도 교수 장 정 식

이 논문을 공학석사 학위논문으로 제출함

2014 년 2 월

서울대학교 대학원

화학생물공학부

장 윤 선

장윤선의 석사 학위논문을 인준함

2014 년 2 월

위 원 장 _____ (인)

부위원장 _____ (인)

위 원 _____ (인)

학위논문 원문제공 서비스에 대한 동의서

본인의 학위논문에 대하여 서울대학교가 아래와 같이 학위논문 제공하는 것에 동의합니다.

1. 동의사항

① 본인의 논문을 보존이나 인터넷 등을 통한 온라인 서비스 목적으로 복제할 경우 저작물의 내용을 변경하지 않는 범위 내에서의 복제를 허용합니다.

② 본인의 논문을 디지털화하여 인터넷 등 정보통신망을 통한 논문의 일부 또는 전부의 복제.배포 및 전송 시 무료로 제공하는 것에 동의합니다.

2. 개인(저작자)의 의무

본 논문의 저작권을 타인에게 양도하거나 또는 출판을 허락하는 등 동의 내용을 변경하고자 할 때는 소속대학(원)에 공개의 유보 또는 해지를 즉시 통보하겠습니다.

3. 서울대학교의 의무

① 서울대학교는 본 논문을 외부에 제공할 경우 저작권 보호장치(DRM)를 사용하여야 합니다.

② 서울대학교는 본 논문에 대한 공개의 유보나 해지 신청 시 즉시 처리해야 합니다.

논문제목 : 엽산수식 실리카-티타니아 중공구조 구형나노입자로 표적화된 MCF-7 세포에 대한 광역동치료

학위구분 : **석사** □ · **박사** □
학 과 : 화학생물공학부
학 번 : 2012-22585
연 락 처 :
저 작 자 : 장윤선 인)
제 출 일 : 2014 년 1 월 30 일

서울대학교총장 귀하

Agreement of Thesis Disclosure
(Do not include this English form in the thesis copy. Use the Korean form in the previous page.)

I approve the thesis distribution service offered by Seoul National University under the following agreement.

1. Agreement

① I approve the duplication of the thesis for the purpose of archiving or online service via internet as long as the contents of the thesis are not modified.
② I approve free duplication, distribution, and transmission of the entire (or partial) thesis in digital format via internet or similar network.

2. Author Responsibility

When the copyright of the thesis is transferred to others or is allowed to be published for any reason that may invalidate this agreement, I will immediately notify the College to defer or stop distributing the copyrighted contents.

3. University Responsibility

① The University must protect the copyright of the thesis under digital rights management (DRM) when providing the thesis to outside individuals or parties.
② The University must process the request for the deferment or suspension of the thesis distribution immediately.

Thesis Title : Folic Acid Conjugated Silica-titania Hollow Nanoparticle Targeting MCF-7 Cells for Photodynamic Therapy

Degree : **Master's □ Ph.D. □**

Department : School of Chemical and Biological Engineering
Student number: 2012-22585
Contact info:
Author name: Yoonsun Jang (Stamp)

Submission date : 2014 년 1 월 30 일
Attn: President of Seoul National University

Abstract

Folic Acid Conjugated Silica-titania Hollow Nanoparticle Targeting MCF-7 Cells for Photodynamic Therapy

Yoonsun Jang

School of Chemical and Biological Engineering

The Graduate School

Seoul National University

Folic acid conjugated SiO_2/TiO_2 hollow nanoparticle (FA-HNP) with 50 nm were fabricated using dissolution and re-deposition method, and encapsulated protoporphyrin IX (PpIX) as photosensitizer for photodynamic therapy of cancer. The FA-HNP-PpIX exhibited excellent mono-dispersity and high loading efficiency of PpIX, and is able to generate cytotoxic singlet oxygen under visible light excitation for photodynamic therapy (PDT). In

order to confirm the targeting effects of folic acid, two human breast cancer cell lines, MCF-7 (folate receptor positive) and SK-BR-3 (folate receptor negative), are used as experimental and control cell line. When MCF-7 cells are treated with FA-HNP-PpIX and irradiated, the viability is decreased to 25.5 %, which is 40 times higher PDT effeciency than that of other PpIX based experiment. On the other hand, in SK-BR-3, there is no significant effect even under irradiation condition. Judging from these data, FA-HNP-PpIX is very suitable for PDT application. A FA-HNP-PpIX system proposes a new possibility to facilitate the implementation of hydrophobic photosensitizer for effective PDT treatment for tumor cells with folate receptor, and can be expanded to practical applications with further studies.

Keywords: Anticancer therapy, Active targeting, Drug delivery system, Hollow nanoparticle, Photodynamic therapy.

Student Number: 2012-22585

List of Figures

significant difference from negative control. (white: no irradiation , gray: irradiated for 15 min)

Figure 18. TEM images of particle-internalized MCF-7 cells and SK-BR-3 cells were incubated with HNP or FA-HNP-PpIX for 24 h: a) MCF-7 cell with HNP, b) MCF-7 cell with FA-HNP-PpIX, c) SK-BR-3 cell with HNP and d) SK-BR-3 cell with FA-HNP-PpIX (MCF-7 and SK-BR-3 cells were incubated at the equivalent 20 μg mL^{-1} HNP concentration). Red arrows indicate the location of HNP and FA-HNP-PpIX.

Figure 19. Live cell fluorescent images of MCF-7 cells and SK-BR-3 cells. Cells were stained with Rh-123 for visualizing the mitochondrial membrane potential of cells. Bothe cells were treated with 60 μg mL^{-1} concentration of FA-HNP-PpIX irradiation time is 15min after 24 h incubation. (Scale bars: 30 μm).

Figure 20. ROS production was measured by a) MCF-7 cells and b) SK-BR-3 cells after incubation with different concentration of FA-HNP-PpIX (10, 20, 30, 40, 50, and 60 μg mL^{-1}) for 24 h. After incubation of FA-HNP-PpIX, cells were irradiated for 15 min. ROS production by c) MCF-7 cells and d) SK-BR-3 cells after treated with 60 μg mL^{-1} of FA-HNP-PpIX for 24 h. After introduction of FA-HNP-PpIX, cells were irradiated with different time scale (0, 5, 10, and 15 min).ROS values were analyzed by flow cytometry. Values exhibit mean ± SD and each experiment was performed in triplicate. *Statistically significant difference from negative control.(white: no FA-HNP-PpIX used as a negative control, gray: incubated with FA-HNP-PpIX, black: incubated with 0.2 % H_2O_2 used as a positive control)

List of Abbreviations

ABDA: 9,10-anthracenediyl-bis(methylene) dimalonic acid

CSNP: core/shell nanoparticle

DMSO : dimethyl sulfoxide

FA: folic acid

FACs: flow cytometry

FR: folate receptor

FT-IR: Fourier transform-infrared

GPTS: γ-glycidoxy propyl trimethoxysilane

HNP: hollow nanoparticle

LED: light emitting diode

PBS: phosphate buffered saline

PDT: photodynamic therapy

PpIX: protoporphyrin IX

PI: propidium iodide

PS: photosensitizer

Rh-123: Rhodamine-123

ROS: reactive oxygen species

TEM: Transmission electron microscopy

TEOS : tetraethyl orthosilicate

TTIP: titanium (IV) isopropoxide

UV-Vis: Ultraviolet-visible

List of Tables

Contents

Chapter 1. Introduction

1.1 Drug Delivery Systems

The many advances in medicine have lead to lengthened life expectancies and significant improvements in our general health conditions. Notably, research in pharmaceutical sciences has played a crucial role in this progress. From ancient Egyptian, Indian and Chinese herbal remedies to state-of-the-art monoclonal antibody-based therapeutics, both synthetic and naturally-occurring chemical or biological compounds have helped mankind fight and defend against diseases for many generations.[1] Recently, the emergence of biotechnology research has generated great interest in developing novel drug delivery systems (DDSs) to improve both the pharmacological and therapeutic properties of parenterally administered drugs.[2, 3] In particular, advances in nanotechnology have produced an array of nanoscaled polymeric, liposomal and inorganic materials as potential drug carriers (Figure 1).[4-6]

The therapeutic applications of nanomaterials have been a boon in medical field by delivering drugs to specific cells. The overall drug consumption and side effects can be lowered significantly by depositing the active agent in the morbid region only and in no higher dose than needed. This highly selective approach reduces costs and human suffering. Unlike large-scale DDSs, nanomaterial-based DDSs (nano-DDSs) offer easier penetration through certain regions of the body due to their small size simplicity in surface modification and, in some cases, multifunctional capabilities for simultaneous therapeutic and imaging applications.[7, 8] The flexible surface chemistry of nano-DDSs also allows the ability to conjugate targeting ligands. Biological moieties such as antibodies, peptides and oligonucleotide sequences can b e attached to their surfaces to target drugs to specific diseased sites.[9]

Within the human body, targeted nano DDS delivery can increase drug payload while significantly reducing the risk of adverse systemic side effects, leading to better patient compliance and enhanced therapeutic efficacy.[10] Furthermore, the ability to alter the size, shape and composition of nanostructures during synthesis has significant implications for present drug delivery strategies.

To address the challenges of targeting tumors with nanotechnology, it is necessary to combine the rational design of nanocarriers with the fundamental understanding of tumor biology. Ideally, for anticancer drugs to be effective in cancer treatment, they should first, after administration, be able to reach the desired tumor tissues. Second, after reaching the tumor tissue, drugs should have the ability to selectively kill tumor cells without affecting normal. These two basic strategies are also associated with improvements in patient survival and quality of life by increasing the intracellular concentration of drugs and reducing dose-limiting toxicities simultaneously. Increasingly, nanoparticles seem to have the potential to satisfy both of these requirements for effective drug carrier systems. A drug delivery system comprising a binary conjugate (i.e., polymer-drug conjugate) that depends only on passive targeting mechanisms inevitably faces intrinsic limitations to its specificity. One approach suggested to overcome these limitations is the inclusion of a targeting ligand or antibody.[11]

Ideally, cell-surface antigens and receptors should have several properties that render them particularly suitable tumor-specific targets. First, they should be expressed exclusively on tumor cells and not expressed on normal cells. Second, they should be expressed homogeneously on all targeted tumor cells. Last, cell-surface antigens and receptors should not be shed into the blood circulation. Whether targeted conjugates can be internalized after binding to target cells is an important criterion in the selection of proper targeting ligands. Internalization usually occurs via receptor-mediated endocytosis (Figure 2).

A folic acid (FA) targeted conjugate binds with folate receptor (FR) on the cell surface, the invaginating plasma membrane envelopes the complex of the receptor and ligand to form an

endosome. The FR is a well-known tumor marker that binds FA and FA-drug conjugates with a high affinity and carries these bound molecules into the cells via receptor mediated endocytosis.[12] FA has high binding affinity ($K_d=10^{-10}$) to FR and thus is useful as targeting ligand to certain types of cancer cells.[13] They have been applied to drug delivery systems as a ligand to enhance selectivity.[14] Ligand-targeted strategies, especially those using receptor-targeting ligands, may have particular potential for overcoming drug resistance because these ligands are usually internalized via receptor-mediated endocytosis, leading to high intracellular drug concentrations (figure 2). Indeed, a FR–targeted nanoparticles exhibited greater inhibitory activity against drug-resistant MCF-7 cells and xenografts than their non targeted free drug counterparts.[15]

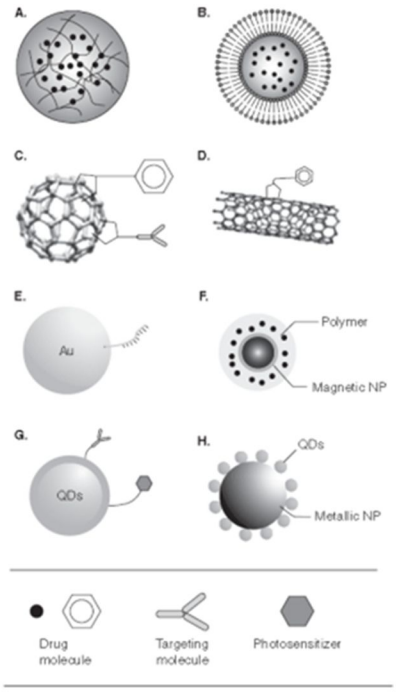

Figure 1. Various nanomaterial-based drug delivery platforms. A. Polymeric nanoparticles/micelles B. Liposome C. Buckyball D. Carbon nanotube E. Colloidal gold nanoparticle F. Magnetic nanoparticle G. Quantum dots H. Multifunctional nanoparticle with metallic nanoparticle core (metallic nanoparticle) and semiconductor quantum dots surrounding the shell. (CNT: Carbon nanotube; NP: Nanoparticle; QD: Quantum dot)

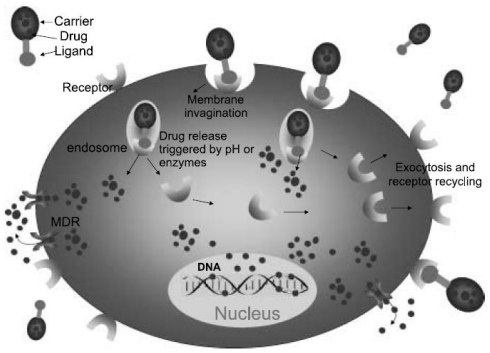

Figure 2. Internalization of nanoparticles via receptor-mediated endocytosis. Tumor-specific ligands or antibodies on the nanoparticles bind to cell-surface receptors, which trigger internalization of the nanoparticles into the cell through endosome.

1.2 Photodynamic Therapy

Photodynamic therapy (PDT) has been received great attention as an alternative to conventional chemotherapy for cancer treatment. PDT involves two individually non-toxic components that are combined to induce cellular and tissue effects in an oxygen-dependent manner (Figure 3).[16]

The first component of PDT is photosensitizer: a photosensitive molecule that localizes to a target cell and tissue. The second component involves the administration of light of a specific wavelength that activates the sensitizer. The photosensitizer transfers energy from light to molecular oxygen, to generate reactive oxygen species (ROS).[17] These reactions occur in the immediate locale of the light-absorbing photosensitizer. Therefore, the biological responses to the photosensitizer are activated only in the particular areas of tissue that have been exposed to light.

One advantage of PDT is that the photosensitizer can be administered by various means, such as by intravenous injection or topical application to the skin. However, biodistribution changes over time, the timing of light exposure is another way to regulate the effects of PDT. Following the absorption of light (photons), the sensitizer is transformed from its ground state (singlet state) into a relatively long-lived electronically excited state (triplet state) via a short-lived excited singlet state.[18] The excited triplet can undergo two kinds of reactions. It can react directly with a substrate, such as the cell membrane or a molecule, and transfer a hydrogen atom (electron) to form radicals. These radicals interact with oxygen to produce oxygenated products and form singlet oxygen. Because the effects of almost all PDT drugs are oxygen dependent, photosensitization typically does not occur in anoxic areas of tissue. Because of the high reactivity and short half-life of the ROS, only cells that are proximal to the area of the ROS production are directly affected by PDT.[19]

The rationale for the use of molecular delivery systems for photosensitizers is similar to that for the delivery of chemotherapeutics and toxins. Carrier-mediated delivery allows increased

accumulation of sensitizer at the targeted site and the use of photosensitizers that have efficient photochemistry but cannot accumulate in tumors adequately. Carriers therefore broaden the clinical repertoire of sensitizers, and minimize the amount of precision that is needed in light delivery. Furthermore, the sensitizer does not need to dissociate from carriers for activation to occur, and additional target specificity can be achieved by controlling the location at which light activates the drug. Various delivery systems have been tested in preclinical models. [20, 21] Ligands against receptors that are upregulated in tumor cells could be delivery vehicle.

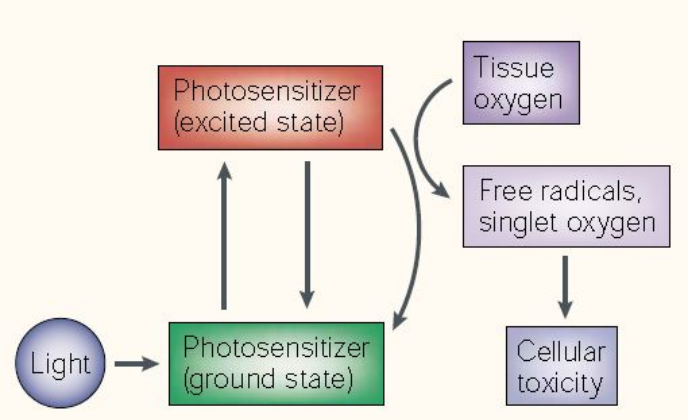

Figure 3. Mechanism of action of photodynamic therapy (PDT). PDT requires three elements: light, a photosensitizer and oxygen. When the photosensitizer is exposed to specific wavelengths of light, it becomes activated from a ground to an excited state. As it returns to the ground state, it releases energy, which is transferred to oxygen to generate reactive oxygen species (ROS), such as singlet oxygen and free radicals. These ROS mediate cellular toxicity.

1.3 Hollow nanoparticles

Hollow structured nanoparticle has attentioned in drug delivery systems. The void space of hollow nanostructure could lead to low density, large specific area, modulate refractive index, mechanical and thermal stabilities, and surface permeability. Furthermore, the large fraction of void space in hollow nanoparticles can be used as a carrier for controllable release of drugs in the pharmaceutical fields.

Among various hollow nanoparticles, hollow mesoporous silica nanoparticles (HMSNs) for biomedical purposes, including drug delivery, have gained increasing interest for use in vaccines. HMSNs have unique structural features, including large surface areas, tunable pore sizes, and well-defined surface properties; these properties indicate that they can be used as carriers for therapeutic compounds in vitro and in vivo. In addition, HMSNs have been approved by the Food and Drug Administration as a new biocompatible material. HMSNs show multifunctional surface modification, controlled release capability, and good thermal stability. Thus, they are ideal nonviral carriers for gene/drug delivery. Furthermore, the low toxicity and degradation properties of porous Si have generated much interest in its use in controlled drug delivery systems. Providing a controlled and localized release of therapeutics within the body are key objectives for increasing efficacy and reducing the risks of potential side effects.[30, 31] Also, the high porosity, and the relatively convenient surface chemistry has spurred interest in the use of this system as a host, or “mother ship” for therapeutics, diagnostics, or other types of payloads. Various approaches to load a molecular payload into a porous Si host have been explored.

Many methods for the preparation of porous silica have been reported. An emerging theme in porous Si as applied to medicine has been the construction of particles that can carry a molecular or a drug. Porous Si can carry cargo such as proteins, enzymes, drugs, or genes.[27, 28] In addition, the optical properties of nanocrystalline silicon can be recruited to perform various therapeutic or

diagnostic tasks for example, quantum confined silicon nanostructures can act as photosensitizers to produce singlet oxygen as a photodynamic therapy.[29] A long-term goal is to harness the optical, electronic, and chemical properties of porous Si that can allow the particles to home to diseased tissues such as tumors and then perform various tasks in vivo. These tasks include detecting, identifying, imaging, and delivering therapies to the tissue of interest.

1.4 Objective of this study

Herein, folic acid (FA) conjugated HNP with 50 nm in diameter was fabricated for PpIX delivery agent to FR-overexpressed MCF-7 cell. We investigate in vitro studies of the PDT effect on both human breast cancer cell lines: MCF-7 (FR-positive; FR+ cancer cells) and SK-BR-3 (FR-negative; FR- cancer cells). The release of PpIX in HNP is observed, and the dark and photo cytotoxicity of the protoporphyrin IX loaded FA conjugated HNP (FA-HNP-PpIX) were evaluated. To maximize the PDT effect, these several strategies were combined: 1) FA was used as targeting ligand for active targeting, 2) 50 nm sized HNP was synthesized for efficient passive targeting and exploited to load large amount of drug, 3) HNP is transparent and no absorption in visible light region, and 4) LED light was used as light source for destructing cancer cells at a specific site, while minimizing undesired normal cell damages.

Chapter 2. Experimental

2.1 Materials

The following chemicals were purchased and used as received: Tetraethyl orthosilicate (TEOS; Aldrich), Pure ethanol (Aldrich), Ammonium hydroxide solution (Samchun), Titanium (IV) isopropoxide (TTIP; Aldrich), protoporphyrin IX (PpIX; Aldrich), γ-glycidoxy propyl trimethoxysilane (GPTS; Aldich), and folic acid (FA; Aldrich)

2.2 Fabrication of FA-HNP-PpIX

Silica nanoparticles were synthesized according to the Stöber method.[32] First, 2.9 mL of TEOS were mixed with ethanol (79 mL), ammonium hydroxide solution (3.9 mL), and water (1.4 mL). The mixture was stirred in a vessel for 12 h under 40 °C temperature for synthesizing silica nanoparticles. Subsequently, 3 mL of TTIP was added into the above mentioned solution. The solution was stirred for 12 h at room temperature. The resultant solution was added into 12 mL of ammonium hydroxide solution and sonicated for 12 h. In order to load the PpIX into the dispersed HNP solution, the PpIX was dissolved in DMSO at a concentration of 10 mg mL^{-1} and 2 mg of HNP was added. The mixture was stirred overnight, and then dried under vacuum. The GPTS (1 mL) were introduced into ethanol solution with HNP-PpIX for overnight. Following, 100 mg of FA was added and stirred overnight. The solution was thoroughly washed to remove unreacted FA.

2.3 Characterization

Transmission electron microscopy (TEM) images were obtained with a JEOL EM-2000 EX II microscope. The surface charge (zeta potential) and size distribution of HNPs were measured by ELS-8000 (Otsuka Electronics, Japan). The BET surface area and average pore volume was analyzed by ASAP 2000 (Micromeritics, USA). Fourier transform infrared (FTIR) spectra were obtained using a FT-IR Frontier (PerkinElmer, USA) in absorption mode at a resolution of 64 cm^{-1}. Ultraviolet-visible (UV-Vis) spectra were acquired using a Lambda-20 spectrometer (PerkinElmer, USA). Photoluminescent absorption spectra were gained with JASCO FP-6500 spectrofluorometer.

2.4 Drug loading efficiency

After loading PpIX in HNP and centrifugation, the supernatant was collected and the residual PpIX amount was measured by UV-vis spectrometry. The drug loading capacity was calculated by **Equation (1)**.

$$\text{Drug loading}\ (\%) = \frac{m_{total} - m_{residual}}{m_{HNP-PpIX}} \times 100 \qquad (1)$$

Where m_{total} is total mass of PpIX and $m_{residual}$ is mass of residual PpIX in the supernatant. $m_{HNP-PpIX}$ is mass of PpIX loaded into HNP.

2.5 Detection of ROS generation

Reactive oxygen species (ROS) generated by PpIX were detected by 9,10-anthracenediyl-bis(methylene) dimalonic acid (ABDA; Aldrich). ABDA can react with singlet oxygen and causes a decrease of ABDA absorption peak at 380 nm. The solution of free PpIX and FA-HNP-PpIX were

prepared by dispersing in 0.1 M phosphate buffered saline (PBS) (equivalent concentration of PpIX). ABDA (10 μL of 50 μg mL^{-1}) was added to 3 mL of FA-HNP-PpIX and free PpIX solutions, separately. Then, the mixture was irradiated with visible light. As a light source, 5W LED light Lantern (ING, China) was used. The generation of singlet oxygen was monitored by recording the decrease in ABDA absorption peak in different irradiation time scale.

2.6 Cell culture

Human breast cancer MCF-7 and SK-BR-3 cell lines were purchased from American Type Culture Collection (ATCC, Manassas, VA, USA). They were cultured with RPMI-1640 medium with 10% fetal bovine serum, and 1% penicillin-streptomycin solution in a 5% CO2 incubator at 37 °C. Cells were placed in 75T flask and maintained between 1×10^5 and 1×10^6 cells mL^{-1}.

2.7 Cell viability assay

The viability of cells treated with FA-HNP-PpIX was measured by using dye exclusion method. This vital stain method uses a 0.4% trypan blue solution (Aldrich). The viable cells were not stained by trypan blue solution. On the other hand, non-viable cells were stained by this solution and classified as dead cells. To perform the assay, cells were cultivated in cover slip placed in 12-well plates (Nunc, Thermo Fisher Scientific, USA) at a density of 7x103 cells per well and incubated for 24 h. Then, cells were treated with FA-HNP-PpIX (10, 20, 30, 40, 50, and 60 μg mL^{-1}) for 24 h. In order to remove the unbound FA-HNP-PpIX, culture medium was removed and cells were washed with 0.1 M Hank's Balanced Salt Solution (HBSS). Subsequently, cells were irradiated with different time scale (0, 5, 10, and 15 min). The irradiated cells were stained with trypan blue solution and observed by

optical microscope (Eclipse E600, Nikon). Cell viability was determined as the percentage of the unstained cells over the untreated cell control.

2.8 Live cell optical microscope observation

Cells were plated at a density of 5000 cells per well in 8-well Lab-Tek II chambered cover glass (Nunc, Thermo Fisher Scientific, USA) and treated with FA-HNP-PpIX (10, 20, 30, 40, 50, and 60 μg mL^{-1}) for 24 h. After treatment, propidium iodide (PI; Vybrant apoptosis kit, Molecular Probes, Invitrogen, Grand Island, NY) staining was carried out. Live cell fluorescent images were obtained by using a Delta Vision RT imaging system (Applied Precision, Issaquah, WA) and Cascade II electron-multiplying charge-coupled device (EMCCD) camera. Dead cells were distinguished by using a fluorescence microscope with appropriate filters. The PI was excited by a wavelength of 535 nm. Viable cells do not exhibit any fluorescence due to the impermeability of dye while dead cells exhibit red fluorescence.

2.9 Cellular uptake of FA-HNP-PpIX

The cellular uptake of HNPs and FA-HNP-PpIX in MCF-7 and SK-BR-3 cells were observed by using transmission electron microscopy (TEM). Both cells were seeded in culture dishes (Nunc, Thermo Fisher Scientific, USA) and cultivated for 24 h. After incubation of HNP and FA-HNP-PpIX (20 mg mL^{-1}) for 24 h, cells were fixed by using Karnovsky's fixative (mixed with 2% paraformaldehyde and 2% glutaraldehyde) for 2 h at 4 °C. Samples were washed with distilled water and post-fixation was conducted by using 1% osmium tetraoxide at 4 °C for 2 h. The samples were

washed with 0.1 M PBS and stained with 0.5% uranyl acetate. Then, ethanol and propylene oxide were used for dehydration of the samples. Cells were embedded in Spurr's resin and sliced by ultramicrotome. The samples were observed by TEM (JEM1010, JEOL) at 80 kV.

2.10 Alteration of mitochondrial membrane potential

To investigate the change of the mitochondrial membrane potential, cells were seeded in 8-well Lab-Tek II chambered cover glass (Nunc, Thermo Fisher Scientific, USA) at a density of 4000 cells per well and treated with FA-HNP-PpIX (60 μg mL^{-1}). After incubation, the cells were stained with 10 μM Rhodamine-123 (Rh-123; Invitrogen, Grand Island, NY). Rh-123 is a specific dye that can directly act on mitochondria. Delta Vision RT imaging system (Applied Precision, Issaquah, WA) equipped Cascade II electron-multiplying charge-coupled device (EMCCD) camera was used to get live cell fluorescent image. Rh-123 dye was excited by a wavelength of 505 nm and emitted 560 nm green fluorescence.

2.11 Quantification of ROS generation by flow cytometry

Reactive oxygen species (ROS) generation in cells was observed by MitoSOX^{TM} Red (Invitrogen, Grand Island, NY) staining followed by flow cytometric measurement of the fluorescence. Cells were incubated in sterile culture dishes (Nunc, Thermo Fisher Scientific, USA) at a density of 5×105 per dish and incubated for 24 h. Then, cells were treated with FA-HNP-PpIX (10, 20, 30, 40, 50, and 60 μg mL^{-1}) for 24 h. After washing with 0.1 M PBS, cells were suspended in 0.1 M HBSS, stained with MitoSOX^{TM} Red, and analyzed by flow cytometry (FACs Aria, BD Bioscience, USA).

Chapter 3. Results and discussion

3.1 Characterization of FA-HNP-PpIX

The overall synthesis process of the FA-HNP-PpIX is shown in Figure 4. Silica nanoparticles were fabricated by Stöber method.[32] By adding TTIP to the silica nanoparticles, titania layers were introduced onto the surface of the silica nanoparticles. HNP was made up by adding silica/titania core/shell nanoparticle into ammonium hydroxide (NH_4OH) solution. Ammonium hydroxide solution can dissolve silica core and redeposit silica on the surface of titania shell.[33] Then, HNP and PpIX were mixed in dimethyl sulfoxide (DMSO) and stirred for 24 h to encapsulate PpIX into HNP (HNP-PpIX). After loading PpIX into HNP, surface of the HNP was pre-modified with GPTS; GPTS-HNP-PpIX and then post-modified with FA (FA-HNP-PpIX). FR is overexpressed on MCF-7 human breast cancer cells and has high binding affinity with FA, which allows FA as a targeting ligand for MCF-7 cells.[34, 35]

Transmission electron microscopy (TEM) images and electrophoretic light scattering spectrophotometer (ELS) data verify HNP had an average diameter of 44.8 nm with narrow size distribution (Figure 5a). After FA treatment, diameter of the HNP was increased by 20 nm while the dispersity and uniformity in size and shape were still remained (Figure 5b). FA functionalized HNP was termed as FA-HNP. From zeta potential (ζ-potential) analysis, the ζ-potential for HNP in deionized water was +0.4 mV. On the other hand, FA-HNP had a ζ-potential of -5.88 mV due to amino group on the surface. The change in the ζ-potential

indicates successful introduction of FA on the surface of the HNP. These synthesis process was confirmed by fourier transform infrared spectroscopy (FT-IR) analysis in Figure 6. FT-IR spectrum of the HNP showed their characteristic peaks at 952 cm^{-1}, 1075 cm^{-1}, and 1402 cm^{-1} corresponding to Si-O-Ti vibration, Si-O stretching and Si-O overtone.[36-38] HNP-PpIX showed C-N stretching at 1076 cm^{-1}, C=O stretching at 1724 cm^{-1} and C=C stretching at 2949 cm^{-1} revealing the presence of PpIX [38-41] The FA mediated surface modification was verified with peak of C-N stretching at 1076 cm^{-1} and C=O stretching at 1724 cm^{-1}.[16, 20] FA-HNP-PpIX observed N-H wagging peak at 732 cm^{-1} and C-N stretching peak at 1261 cm^{-1}. [43, 44] Moreover, the characteristic peak of FA-HNP-PpIX was verified with aromatic C-H vibration at 1261 cm^{-1} and CH_2 rocking vibration of Si-CH_2-R at 698 cm^{-1}. The peak assignments were summarized in **Table S1**.

Figure 7 shows the nitrogen adsorption isotherm and average pore volume of HNP. HNP has a BET surface area of 313 $m^2\ g^{-1}$ and an average pore volume of 0.92 $cm^3\ g^{-1}$. The ROS generated from PpIX effectively diffuse out of the HNP's pore. Furthermore, Large hollow cavity and mesoporous shell of HNP suggests a possible therapeutic application for delivering drugs. To investigete the potential of the HNP as drug delivery agent, the loading capacity was evaluated. Measured by UV-vis spectroscopy, 1.645 μmol of PpIX were loaded in 1 mg of HNP-PpIX. The loading capacity of the HNPs was 40 times higher than that of previous mesoporous system, even though HNP (diameter : 50 nm) was about half the diameter of the mesoporous silica (diameter: 110 nm).[45] This result promises a potential carrier agent for efficient drug delivery.

The UV-vis absorption spectra of FA-HNP-PpIX dispersed in different solvents were

shown in Figure 8. In order to compare the behavior of the FA-HNP-PpIX in different solvents, DMSO and phosphate buffer saline (PBS) were selected. In DMSO, PpIX loaded in FA-HNP-PpIX dissolved as a monomer with a sharp Soret band at 402 nm. PpIX stayed as aggregates in PBS with broadened split Soret band of moderate intensity was observed. Figure 9 indicated PpIX showed bright fluorescence at 632 nm (λex: 402 nm) in DMSO, while aggregated PpIX in aqueous environment exhibited the decrease of fluorescence intensity with a blue shift of emission peak at 620 nm (λex: 402 nm).[46] PpIX was fully dissolved in DMSO and came out of the HNPdue to hydrophobicity. Contrary to DMSO, PpIX was not soluble in PBS and maintained its aggregation inside of the HNP. Therefore, it can be concluded that the PpIX was successfully loaded inside the HNP by solvent exchange methods, and delivered into cancer cells without leakage. This results verify the potential of FA-HNP-PpIX as efficient drug delivery agent.

To confirm release profile of the PpIX from FA-HNP-PpIX, absorption measurement was performed using UV-vis spectroscopy (Figure 10). The release profile of PpIX from FA-HNP-PpIX showed different release pattern depending on the solvents. In DMSO, FA-HNP-PpIX released PpIX about 63.5 %, 69 %, and 100 % after 15 min, 30 min, and 360 min, respectively. However, the FA-HNP-PpIX released very few PpIX in PBS even after 360 min, which might be due to the hydrophobicity of PpIX. Considering these result, FA-HNP could load large amount of PpIX and deliver PpIX effectively to inner phase of cancer cell without leakage, which is suitable for *in vitro* drug release/permeation system.

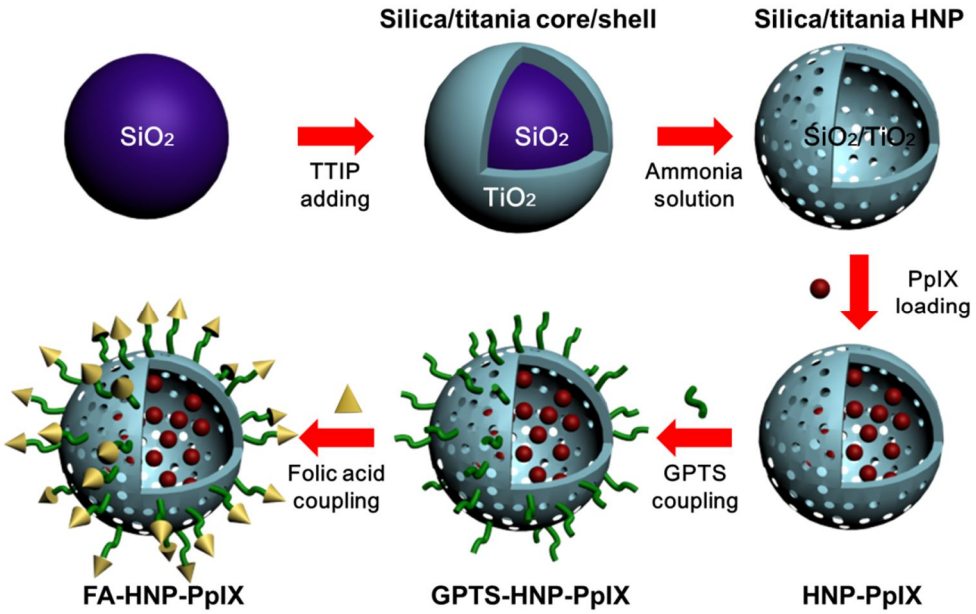

Figure 4. Schematic illustration of fabrication of FA-HNP-PpIX. FA-HNP was used as encapsulating agent for PpIX.

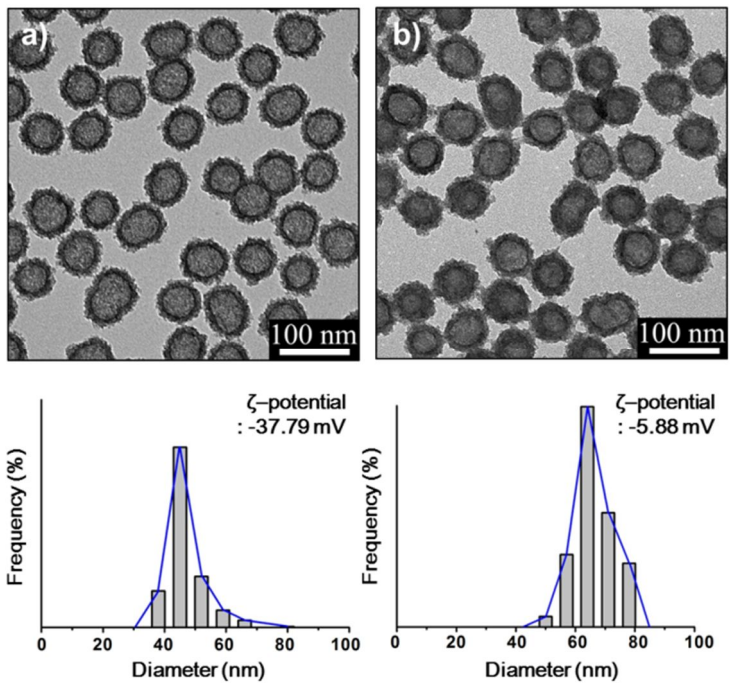

Figure 5. TEM images of a) HNP and b) FA-HNP (below: size distribution histograms and ζ-potential determined by ELS).

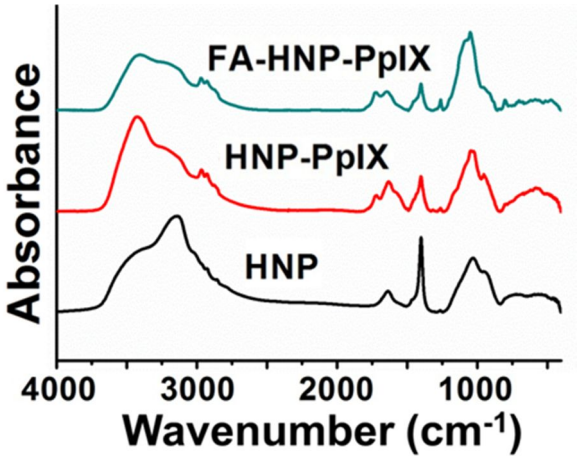

Figure 6. Infrared spectroscopy absorbance spectrum of HNP, HNP-PpIX, and FA-HNP-PpIX.

Table 1. Table S1. FT-IR assignment of materials.

Materials	Wavenumber (cm^{-1})	Assignments
HNP	3239	-OH stretching
	1634	-OH vibration
	1402	Si-O overtone
	1025	Si-O stretching
	952	Si-O-Ti
PpIX	2949	C=C symmetric stretching
	1724	C=O stretching
	1076	C-N stretching
FA	1724	C=O stretching
	1261	aromatic =C-H vibration
	1076	C-N stretching
	698	Si-CH_2-R vibration

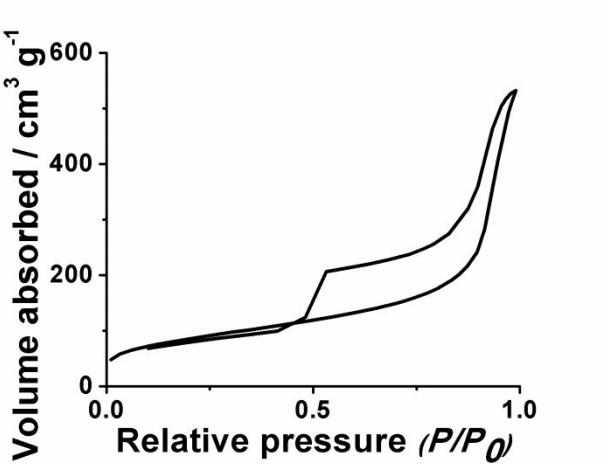

Figure 7. Nitrogen adsorption isotherm of the hollow nanoparticles; pore volume=0.92 $cm^3 g^{-1}$, BET surface area 313 $m^2 g^{-1}$.

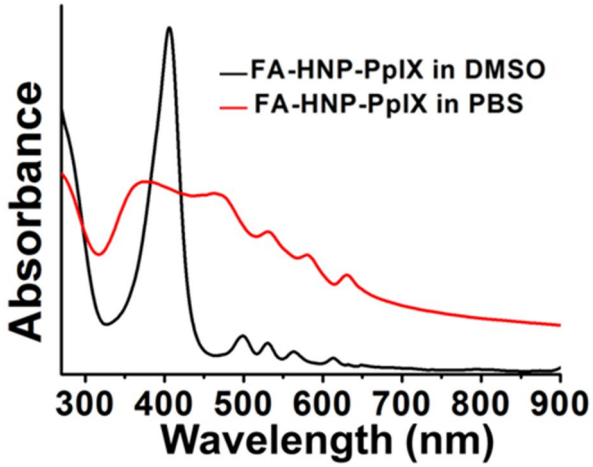

Figure 8. UV-visible spectroscopy absorption spectrum of FA-HNP-PpIX in different solvents.

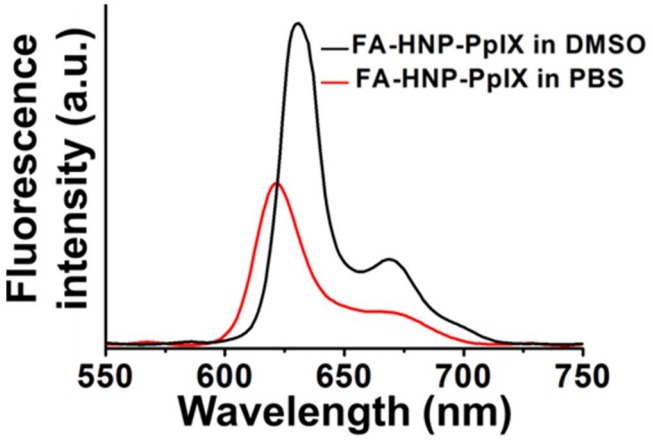

Figure 9. Fluorescence intensity of FA-HNP-PpIX in different solvents.

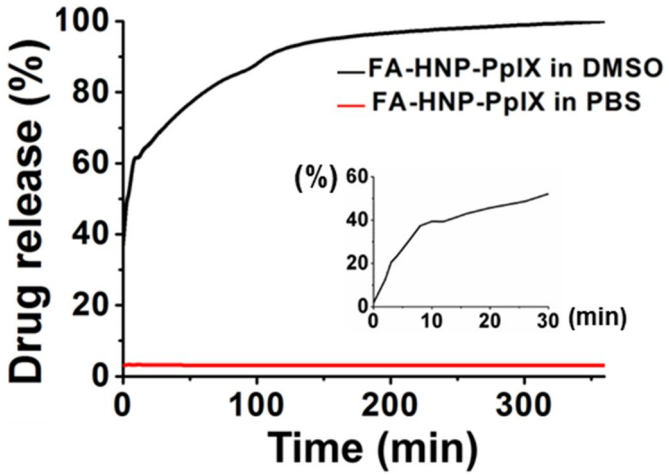

Figure 10. Time dependent cumulative PpIX drug release profile of 0.3 mg mL^{-1} FA-HNP-PpIX.

3.2 Singlet oxygen ($^1O_2$) generation

$^1O_2$ generation efficiency of photosensitizers is important factor in photodynamic therapy.[47] Before the measurement of singlet oxygen generation, the visible light absorption of HNP was investigated for using LED as light source for PDT application. HNP had no absorption in a wavelength range of 400 - 700 nm, indicating LED light penetrate into the HNP without loss, and reacted with PpIX in the HNP (Figure 11). According to previous reports, LED has superior properties to other types of light sources such as intact of healthy cells during irradiation and easy to access in daily life. Therefore, PDT using LED as light source is expected to be more effective and have less side effects.

In order to confirm photodynamic activity of the FA-HNP-PpIX, $^1O_2$ generation was detected by chemical trapping method using 9,10-anthracenediyl-bis(methylene) dimalonic acid (ABDA).[48] ABDA can react with the generated $^1O_2$ to yield, which causes a decrease of ABDA absorption spectra peak at 380 nm.[49, 50] For monitoring the $^1O_2$ generation, the ABDA was dropped into FA-HNP-PpIX and irradiated with different time scale at intervals of 3 min, and other samples were stayed in dark room. Figure 12a showed absorbance spectra of ABDA decreased in solutions containing FA-HNP-PpIX. Based on Figure 12a, time dependent ABDA consumption was calculated under irradiated and non-irradiated condition. The absorption of the irradiated sample decreased, while no significant changes were observed in non-irradiated sample. At 9 min, there is a noticeable difference in absorbance change between irradiated and non-irradiated samples, indicating that photodynamic therapy could be valid at minimum 9 min (Figure 12b) By using ABDA, the effective $^1O_2$ generation from FA-HNP-PpIX was assessed under irradiation, which indicates this system is suitable for destructing cancer cell *via* PDT.

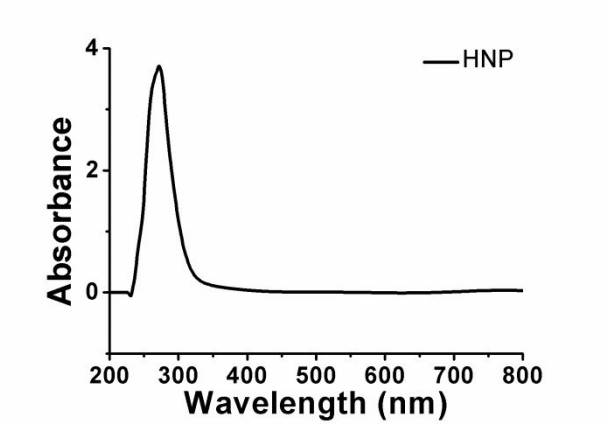

Figure 11. UV/visible absorption spectrum of HNPs in PBS

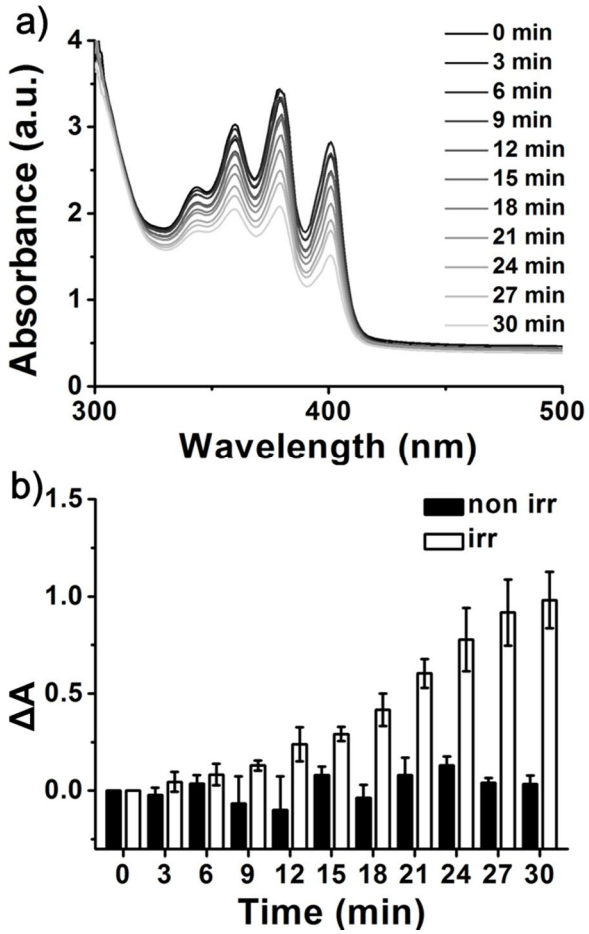

Figure 12. Photobleaching of ABDA (0.07 mg mL^{-1}) by FA-HNP-PpIX (0.2 mg mL^{-1}) nanoparticles dispersed in 0.1 M PBS. a) Absorbance spectra of FA-HNP-PpIX nanoparticles irradiated with different time scale by using visible light. b) The change of absorption intensity of ABDA without light and irradiated FA-HNP-PpIX nanoparticles.

3.3 PDT efficacy of FA-HNP-PpIX

To investigate the mode of cell death and the PDT effect of FA-HNP-PpIX for cancer cell destruction, FA-HNP-PpIX induced phototoxicity was probated by live cell observation. In Figure 13, a schematic outline of the anti-cancer effect of the FA-HNP-PpIX is presented. In this study, the cancer treatment effects were compared using MCF-7 and SK-BR-3 cell lines. Both cell lines are human breast cancer cell lines, but FR was only overexpressed on the MCF-7 cells. The cells were incubated with different concentration of FA-HNP-PpIX and irradiated with different time scale. After FA-HNP-PpIX treatment and irradiation, the dead cells were stained with propidium iodide (PI) which can stain dead cells specifically and exhibit red fluorescence. Figure 14 illustrated that red fluorescence was observed more in MCF-7 cells with the increase of the concentration of FA-HNP-PpIX and the light irradiation time. On the other hand, no noticeable cell death was observed in FR-SK-BR-3 cells even increase of the FA-HNP-PpIX concentration and light irradiation time (Figure 15). These results demonstreated that FA-HNP-PpIX exhibited highly active targeting ability for FR overexpressed cancer cells and excellent photodynamic efficacy.

To quantify the statistical selective photodynamic efficiency on the both cell lines, the viability of the FA-HNP-PpIX-treated cells was determined by trypan blue exclusion method. Viable cells with an intact plasma membrane are not stained, while dead cells become intensely blue.[51] MCF-7 and SK-BR-3 cells were cultivated with FA-HNP-PpIX for 24 h and irradiated with visible light. As shown in Figure 16, the cell viability decreased with the increasing of irradiation time and FA-HNP-PpIX concentrations in both MCF-7 and SK-BR-3, indicating that photodynamic effect can be valid under visible light irradiation. In MCF-7 cells, the degree of cell death was observed up to 74.5 % (at 60 μg mL^{-1} of FA-HNP-PpIX with 15 min irradiation) when irradiated with visible light. Compared to previous reports, an about 20 times lower amount of nanoparticles (50 μg mL^{-1} of FA-HNP-PpIX) and

2 times shorter irradiation time (10 min) were used to achieve the comparative cell death.[52] This result indicates that relatively large amount of PpIX was successfully loaded in FA-HNP-PpIX and delivered to cancer cells, which cause efficient cancer cell destruction. Moreover, the PDT activity on MCF-7 cells was observed to be more effective than on SK-BR-3 cells at the same irradiation time and FA-HNP-PpIX concentration due to active targeting ability of FR. These findings are consistent with live cell observation result. When stored in the dark, the degree of cell death indicated <10%, showing that FA-HNP-PpIX has biocompatibility and low dark toxicity to both cells. The control experiment established that HNPs, FA–HNP, and HNP–PpIX do not induce significant cell death toward MCF-7 and SK-BR-3 with 15-min irradiation. (Figure 17) However, in this experiment, FA–HNP-incubated MCF-7 cells were slightly less viable than SK-BR-3 cells, indicating that the FA–HNP selectively acts on the FR+ MCF-7 cells. These data indicate that the targeting capability of the FA–HNP–PpIX to FR+ MCF-7 cells provides effective and selective tumor destruction and low dark toxicity. Hence, an effective, selective tumor destruction, and safe dark toxicity was demonstrated, indicating that a novel drug delivery and targeting effect of the FA-HNP-PpIX to FR+ MCF-7 cells.

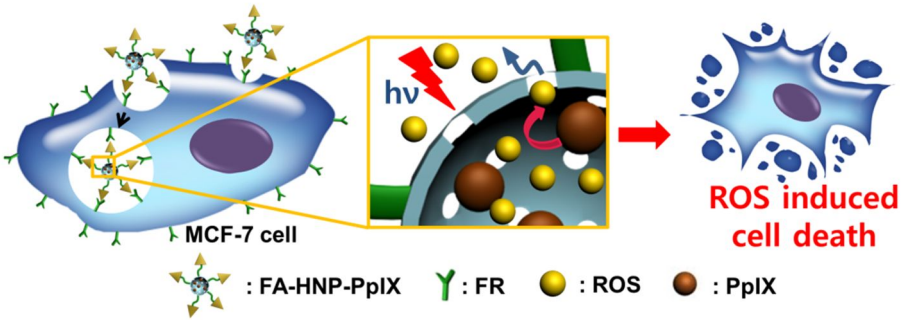

Figure 13. Schematic outline of the anti-cancer effect of the FA-HNP-PpIX

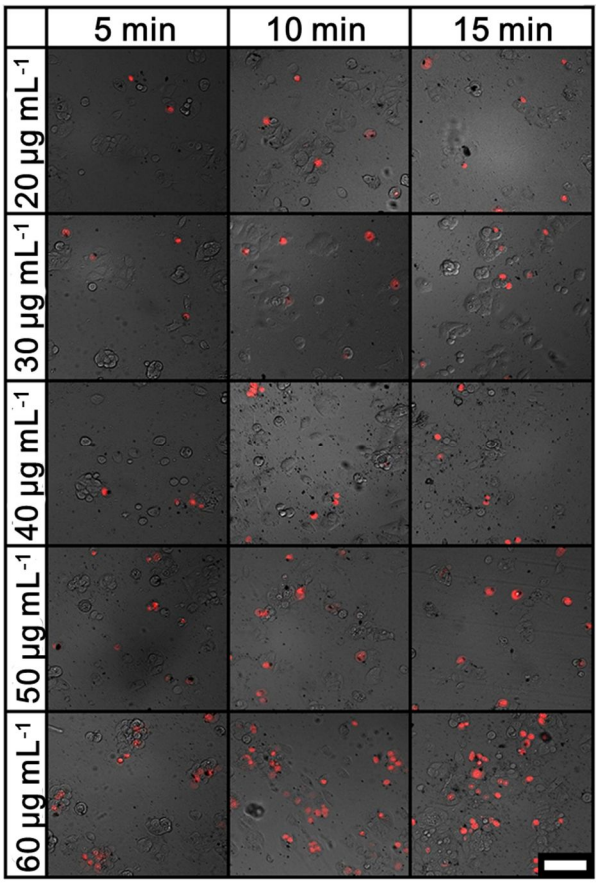

Figure 14. Live cell differential interference contrast (DIC) and fluorescence images of FA-HNP-PpIX treated MCF-7 cell. From up to the bottom, the concentration of FA-HNP-PpIX is 10, 20, 30, 40, 50 and 60 µg mL^{-1}. From left to right, irradiation time is 0, 5, 10, and 15 min. Cells were stained with propidium iodide (PI) for visualing necrosis of cells. DIC images were taken at the same time, corresponding to the fluorescence images (scale bars: 100µm).

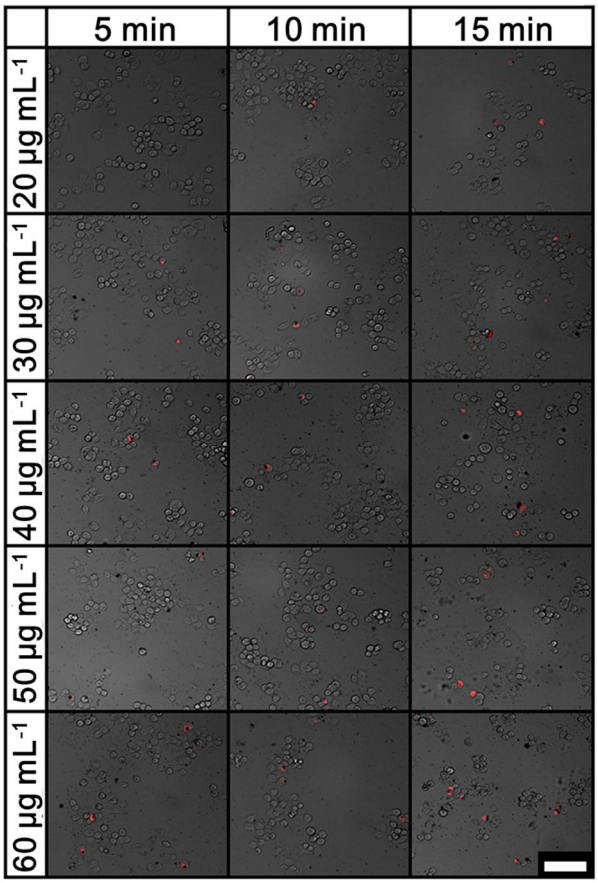

Figure 15. Live cell differential interference contrast (DIC) and fluorescence images of FA-HNP-PpIX treated SK-BR-3 cell. From up to the bottom, the concentration of FA-HNP-PpIX is 10, 20, 30, 40, 50 and 60 μg mL^{-1}. From left to right, irradiation time is 0, 5, 10, and 15 min. Cells were stained with propidium iodide(PI) for visualizing dead cells. DIC images were taken at the same time, corresponding to the fluorescence images(scale bars: 100μm).

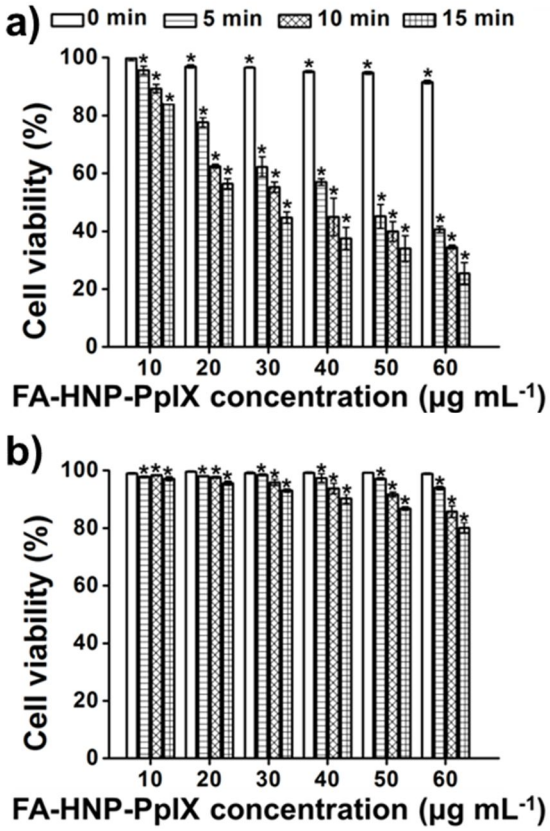

Figure 16. Cell viability of a) MCF-7 and b) SK-BR-3 cells with dose (10, 20, 30, 40, 50, and 60 μg mL^{-1}) and irradiation time dependence (0, 5, 10, and 15 min). Cells were irradiated after 24 h incubation. Values exhibit mean ± SD and each experiment was performed in triplicate. *Statistically significant difference from negative control.

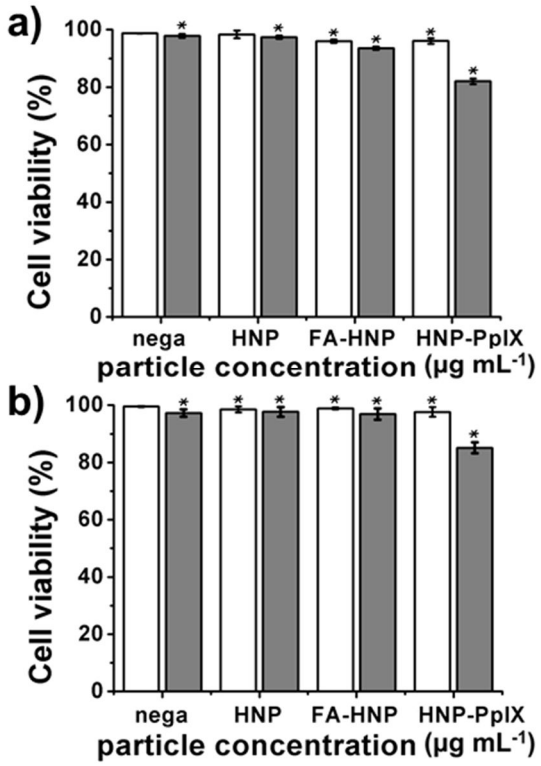

Figure 17. Cell viability of a) MCF-7 and b) SK-BR-3 cells with different particles (HNP, FA-HNP and HNP-PpIX were treated at the equivalent 5 μg mL^{-1} of HNP concentration). Cells were irradiated for 15 min after 24 h incubation. Values exhibit mean ± SD and each experiment was performed in triplicate. *Statistically significant difference from negative control. (white: no irradiation , gray: irradiated for 15 min)

3.4 Cellular uptake of FA-HNP-PpIX

Considering the result of the live cell observation and cell viability test, the PDT effect was dependent on the concentration of the FA-HNP-PpIX. Based on these findings, we hypothesized that intracellular FA-HNP-PpIX concentrationis the the key factor that making difference between MCF-7 and SK-BR-3. The intracellular HNP and FA-HNP-PpIX into SK-BR-3 and MCF-7 were observed by TEM images, and the images showed both particles were internalized into each cell. The intracellular particles are well maintained their original shape, and most of the particles were located inside the endosome. Even after the particle internalization into the cells, it didn't derive serious cell damage and cell toxicity. As shown in Figure 18a and Figure 18c, similar amount of HNP was internalized into SK-BR-3 and MCF-7 cells. On the contrary, Figure 18b and Figure 18d showed FA-HNP-PpIX particle was more internalized into the MCF-7 than into the SK-BR-3. This result strongly supported by the cell viability test (Figure 14, 15, 16 and 17). From this cellular uptake result, the FA mediated targeting stretage could improved selectivity for FR+ MCF-7 cell and induced high intracellular FA-HNP-PpIX concentrationon the FR+ MCF-7 cell, making FA-HNP-PpIX effective for PDT in only FR+ cancer cell.

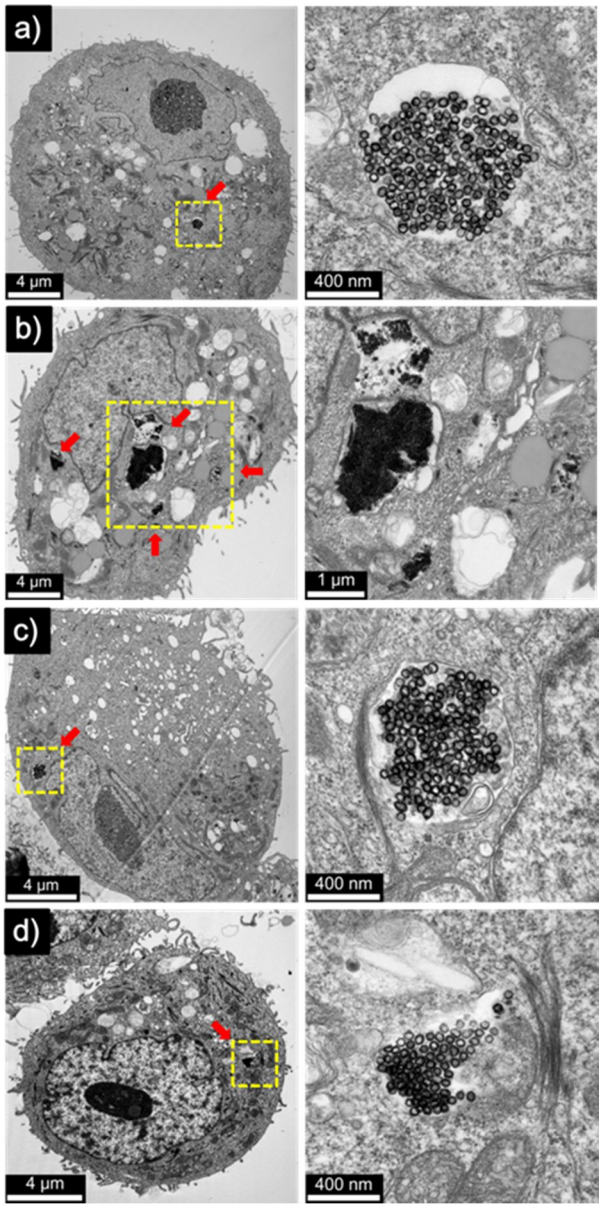

Figure 18. TEM images of particle-internalized MCF-7 cells and SK-BR-3 cells were incubated with HNP or FA-HNP-PpIX for 24 h: a) MCF-7 cell with HNP, b) MCF-7 cell with FA-HNP-PpIX, c) SK-BR-3 cell with HNP and d) SK-BR-3 cell with FA-HNP-PpIX (MCF-7 and SK-BR-3 cells were incubated at the equivalent 20µg mL^{-1} HNP concentration). Red arrows indicate the location of HNP and FA-HNP-PpIX.

3.5 Observation of mitochondrial photodamage

The correlation between the phototoxic cell death and the mitochondrial membrane potential alteration was confirmed by monitoring mitochondrial stress. Reactive oxygen species (ROS) (e.g. singlet oxygen) generated by PDT can lead to the degradation of mitochondrial membrane potential integrity.[53, 54] In this regard, the mitochondrial dysfunction could be an indicator of cell damage and induce efficient cell death.[55] To demonstrate the PDT effect on both cell lines, mitochondrial function was investigated by monitoring the changes of the Rhodamine-123 (Rh-123) fluorescence intensity. Rh-123 is a mitochondrial specific dye and used to investigate the effect of FA-HNP-PpIX on the mitochondrial membrane potential when light was irradiated.[56-58] Through live cell fluorescence image in a time lapse manner, the decrease of mitochondrial membrane potential was observed with 60 μg mL^{-1} of FA-HNP-PpIX at different irradiation time scale (0, 5, 10, and 15 min). In Figure 19, there were significant fluorescence intensity increase and uniformization of the intensity in MCF-7 cells. However, in SK-BR-3 cells, no noticeable fluorescence intensity change was observed. Depolarization or hyperpolarization of the mitochondrial membrane potential induced the increase or reduction of Rh-123 fluorescence intensity, respectively.[59-61] According to increased Rh-123 fluorescence intensity, ROS generated as a result of PDT could be considered as depolarization inducer of mitochondrial membrane potential. This depolarization might be followed by this cell injury step: ROS generated from PDT brings mitochondrial membrane potential damage. This mitochondrial membrane potential damage eventually cause mitochondrial membrane potential depolarization.[62, 63] This result is strongly supported by cell viability test, which is occurred by the high phototoxicity of FA-HNP-PpIX. In addition, heterogeneous Rh-123 fluorescence signal change to homogeneous fluorescence signal, which indicates Rh-123 was released from mitochondria and relocated to cytosol due to cell damage.

Mitochondrial damage was further examined by MitoSOX^{TM} Red. In general, mitochondrial cell damage induce mitochondrial superoxide production.[64] Therefore, the amount of superoxide that occurs in the mitochondria is an indicator of how cells had been damaged.[65] In this study, MitoSOX^{TM} Red was used to examine the degree of the mitochondrial superoxide generation. They can penetrate into living cells, react selectively with mitochondrial superoxide, oxidized by superoxide, and then emitted red fluorescence.[66] As shown in Figrue 20, the amount of superoxide that generated from MCF-7 cells was significantly greater than that of SK-BR-3 cells. The generation of mitochondrial superoxide was increased proportionally to irradiation time and FA-HNP-PpIX concentration in MCF-7 cells. On the contrary, in SK-BR-3 cells, there is no obvious difference in the degree of superoxide generation between negative and FA-HNP-PpIX treated cells. This results are corroborated by the alteration of mitochondrial membrane potnetial generation result presented in Figure 19. The generated mitochondrial superoxide can cause oxidative stress to the cell and eventually lead to cell death. Collectively, under irradiation, ROS generated from FA-HNP-PpIX induced mitochondrial depolarization and these damaged mitochondria produced mitochondrial superoxide. By these process, FR+ MCF-7 cell can be eliminated effectively. Therefore, FA-HNP-PpIX can be considered as promising anticancer agent for FR+ tumor cell.

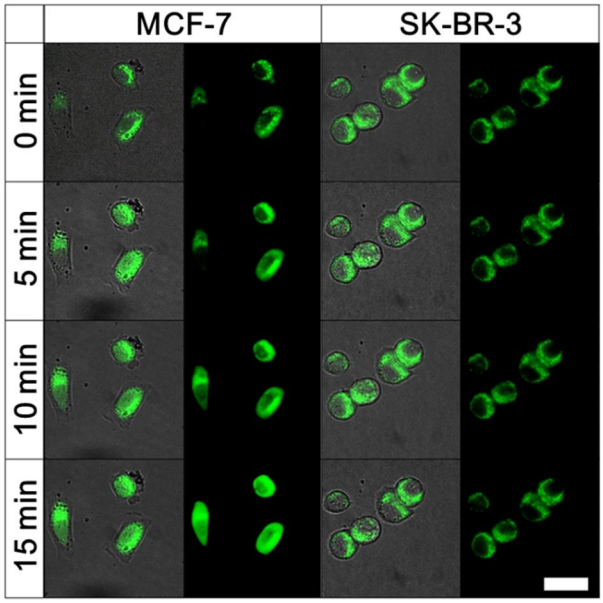

Figure 19. Live cell fluorescent images of MCF-7 cells and SK-BR-3 cells. Cells were stained with Rh-123 for visualizing the mitochondrial membrane potential of cells. Bothe cells were treated with 60 μg mL^{-1} concentration of FA-HNP-PpIX irradiation time is 15min after 24 h incubation. (Scale bars: 30 μm).

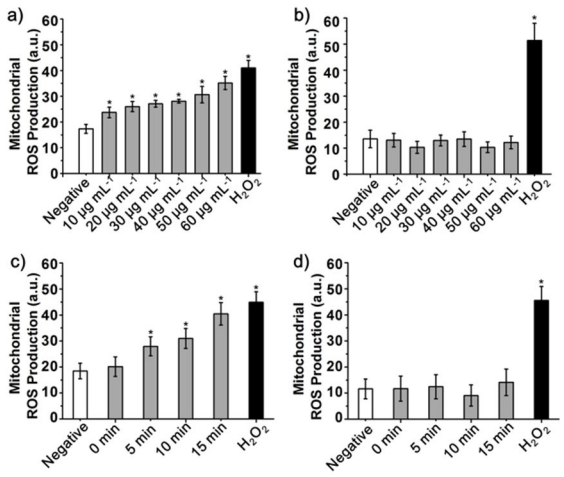

Figure 20. ROS production was measured by a) MCF-7 cells and b) SK-BR-3 cells after incubation with different concentration of FA-HNP-PpIX (10, 20, 30, 40, 50, and 60 μg mL^{-1}) for 24 h. After incubation of FA-HNP-PpIX, cells were irradiated for 15 min. ROS production by c) MCF-7 cells and d) SK-BR-3 cells after treated with 60 μg mL^{-1} of FA-HNP-PpIX for 24 h. After introduction of FA-HNP-PpIX, cells were irradiated with different time scale (0, 5, 10, and 15 min).ROS values were analyzed by flow cytometry. Values exhibit mean ± SD and each experiment was performed in triplicate. *Statistically significant difference from negative control.(white: no FA-HNP-PpIX used as a negative control, gray: incubated with FA-HNP-PpIX, black: incubated with 0.2 % H_2O_2 used as a positive control)

Chapter 4. Conclusion

Monodisperse HNP with 50 nm in diameter were used as a nanocarrier to load photosensitizer PpIX for photodynamic therapy, and their surface was further functionalized with FA for active targeting to FR+ cancer cells. In order to minimize photodamage for normal cells, LED light was used as PDT light source as a replacement of conventional laser. Two breast cancer cell lines were used for identifying active targeting effects of FA; MCF-7 is FR+ and SK-BR-3 is FR- cells. We systematically investigated the effect of FA-HNP-PpIX on phototoxicity, mitochondrial alternation, mitochondrial ROS production, and nanoparticle uptake of both cell lines. At the same experimental condition (60 μg mL^{-1} FA-HNP-PpIX for 15 min irradiation), the MCF-7 cell viability was dropped to 25.5% compared with 80% for SK-BR-3 cells due to FA on HNP. Compared to previous research, FA-HNP-PpIX were 40 times higher efficient PDT effects to achieve the comparative cell death. Therefore, FA-HNP-PpIX system offers a new direction for a photodynamic therapy and can be expanded to practical applications with further studies.

References

[1] Y. XinRong, C. AnMin, M. YingFu, G. Yuan, G. ZheMin, F. BingYi, S. Fang, Q. JinLin, L. Quan, W. ShuQian, *Traditional Chinese medicine. A manual from AZ: symptoms, therapy and herbal remedies* **2003**.

[2] M. A. Moses, H.Brem, R. Langer, *Cancer cell* **2003**, *4*, 337.

[3] D. A. LaVan, T. McGuire, R. Langer, *Nat. Biotechnol.* **2003**, *21*, 1184.

[4] J. Panyam, V. Labhasetwar, *Adv. DrugDdeliv. Rev.* **2012,** *64*, 61.

[5] K. Kataoka, A. Harada, Y. Nagasaki, *Adv. DrugDdeliv. Rev.* **2012,** *64*, 37.

[6] G. Batist, G. Ramakrishnan, C. S. Rao, A. Chandrasekharan, J. Gutheil, T. Guthrie, P. Shah, A. Khojasteh, M. K. Nair, K. Hoelzer, *J. Clin. Oncol.* **2001**, *19*, 1444.

[7] P. Lockman, R. Mumper, M. Khan, D. Allen, *Drug Dev.Ind. Pharm.* **2002**, *28*, 1.

[8] T. J. Yoon, J. S. Kim, B. G. Kim, K. N. Yu, M. H. Cho, J. K. Lee, *Angew. Chem.* **2005**, *117*, 1092.

[9] M. Ferrari, *Nat. Rev. Cancer* **2005**, *5*, 161.

[10] R. Langer, *Nature* **1998**, *392*, 5.

[11] T. M. Allen, *Nat. Rev. Cancer* **2002**, *2*, 750.

[12] C. P. Leamon, J. A. Reddy, *Adv. Drug Deliv. Rev.* **2004**, *56*, 1127.

[13] G. Toffoli, A. Russo, A. Gallo, C. Cernicoi, S. Miotti, R. Sorio, S. Tumolo, M. Boiocchi, *Int. J. Cancer* **1998**, *79*, 121.

[14] O. C. Farokhzad, S. Jon, A. Khademhosseini, T.N.T. Tran, D. A. LaVan, R. Langer, *Cancer Res.* **2004**, *64*, 7668.

[15] S. K. Sahoo, V. Labhasetwar, *Mol. Pharm.* **2005**, *2*, 373.

[16] D. E. Dolmans, D. Fukumura, R. K. Jain, *Nat. Rev. Cancer* **2003**, *3*, 380.

[17] J. H. Epstein, In *Phototoxicity and photoallergy*, Seminars in cutaneous medicine and

surgery, Elsevier, **1999**, 274.

[18] B. W. Henderson, T. J. Dougherty, *Photochem. Photobiol.* **1992**, *55*, 145.

[19] J. Moan, K. BERG, *Photochem. Photobiol.* **1991**, *53*, 549.

[20] Y. N. Konan, R. Gurny, E. Allémann, *J. Photochem. Photobiol. B* **2002**, *66*, 89.

[21] N. Swamy, D. A. James, S. C. Mohr, R. N. Hanson, R. Ray, *Bioorg. Med. Chem.* **2002**, *10* , 3237.

[22] R. T. Collins, P. M. Fauchet, M. A. Tischler, *Phys. Today* **1997**, *50*, 24.

[23] A. Foucaran, F. Pascal Delannoy, A. Giani, A. Sackda, P. Combette, A. Boyer, *Thin Solid Films* **1997**, *297* , 317.

[24] M. J. Sailor, J. R. Link, *Chem. Commun.* **2005**, *11*, 1375.

[25] J. L. Coffer, M. A. Whitehead, D. K. Nagesha, P. Mukherjee, G. Akkaraju, M. Totolici, R. S. Saffie, L. T. Canham, P*hysica Status Solidi A. Appl. Res.* **2005**, *202*, 1451.

[26] L. T. Canham, C. L. Reeves, D. O. King, P. J. Branfield, J. G. Crabb, M. C. Ward, *Adv. Mater.* **1996**, *8* , 850.

[27] J. Salonen, L. Laitinen, A. Kaukonen, J. Tuura, M. Björkqvist, T. Heikkilä, K. Vähä-Heikkilä, J. Hirvonen, V. P. Lehto, *J. Control. Release.* **2005**, *108*, 362.

[28] L. A. DeLouise, B. L. Miller, *Anal. Chem.* **2005**, *77*, 1950.

[29] C. Lee, H. Kim, Y. Cho, W. I. Lee, *J. Mater. Chem.* **2007**, *17* , 2648.

[30] K. Braeckmans, S. C. De Smedt, M. Leblans, R. Pauwels, J. Demeester, *Nat. Rev. Drug Discov.* **2002**, *1*, 447.

[31] I. Brigger, C. Dubernet, P. Couvreur, *Adv. Drug Deliv. Rev.* **2012**, *64*, 24.

[32] W. Stöber, A. Fink, E. Bohn, *J. Colloid interface Sci* **1968**, *26*, 62.

[33] G. Bogush, M. racy, C. Zukoski, *J. Non Cryst. Solids* **1988**, *104*, 95.

[34] M. Wu, W. Gunning, M. Ratnam, *Cancer Epidemiol., Biomarkers Prev.* **1999**, *8* , 775.

[35] J. Sudimack, R. J. Lee, *Adv. Drug Deliv. Rev.* **2000**, *41*, 147.

[36] A. R. Loiola, J. C. R. A. Andrade, J. M. Sasaki, L. R. D. da Silva, *J. Colloid interface Sci* **2012**, *367*, 34.

[37] J. Yao, W. Zhan, X. Liu, Y. Guo, Y. Wang, Y. Guo, G. Lu, *Microporous Mesoporous Mater.* **2012**, *148*, 131-136.

[38] G. Socrates, *Infrared and Raman characteristic group frequencies : tables and charts*. 3rd ed. Wiley: Chichester, New York, **2001**, 347.

[39] N. C. Desai, A. Dodiya, P. Shihora, , *Med. Chem. Res.* **2012,** *21*, 1577.

[40] T. Wu, X. P. Zhang, C. H. Li, P. Bouř, Y. Z. Li, X. Z. You, *Chirality* **2012**, *24*, 451.

[41] J. Avalani, D. Patel, D. Raval, *J. Chem. Sci.* **2012**, *124*, 1091.

[42] A. Ruhal, J. Rana, S. Kumar, A. Kumar, *Cell. Mol. Biol.* **2012**, *58*, 15.

[43] A. Kumar, N. Tarannum, M. Singh, *Mater. Sci. Appl.* **2012**, *3*.

[44] Y. Furukawa, F. Ueda, Y. Hyodo, I. Harada, T. Nakajima, T. Kawagoe, *Macromolecules* **1988**, *21*, 1297.

[45] H. L. Tu, Y. S. Lin, H. Y. Lin, Y. Hung, L. W. Lo, Y. F. Chen, C. Y. Mou, *Adv. Mater.* **2009**, *21*, 172.

[46] H. Ding, B. D. Sumer, C. W. Kessinger, Y. Dong, G. Huang, D. A. Boothman, J. Gao, *J. Control. Release.* **2011**, *151*, 271.

[47] J. F. Lovell, T. W. Liu, J. Chen, G. Zheng, J. Gao, *Chem. Rev.* **2010**, *110*, 2839.

[48] T. Zhao, H. Wu, S. Q. Yao, Q. H. Xu, G. Q. Xu, *Langmuir* **2010**, *26* , 14937.

[49] Z. Li, J. Wang, J. Chen, W. Lei, X. Wang, B. Zhang, *Nanotechnology* **2010**, *21*, 115.

[50] P. Couleaud, V. Morosini, C. Frochot, S. Richeter, L. Raehm, J. O. Durand, *Nanoscale* **2010**, *2*, 1083.

[51] M. Bottini, S. Bruckner, K. Nika, N. Bottini, S. Bellucci, A. Magrini, A. Bergamaschi, T.

Mustelin, *Toxicol. Lett.* **2006,** *160*, 121.

[52] W. Li, W. Lu, Z. Fan, X. Zhu, A. Reed, B. Newton, Y. Zhang, S. Courtney, P. T. Tiyyagura, R. R. Ratcliff, *J. Mater. Chem.* **2012**, *22*, 12701.

[53] J. J. Lemasters, A. L. Nieminen, T. Qian, L. C. Trost, S. P. Elmore, Y. Nishimura, R. A. Crowe, W. E. Cascio, C. A. Bradham, D. A. Brenner, B. Herman, *Biochim. Biophys. Acta, Bioenerg.* **1998**, *1366*, 177.

[54] A. Nieminen, A. Saylor, S. Tesfai, B. Herman, J. Lemasters, *Biochem. J.* **1995**, *307*, 99.

[55] S. Orrenius, V. Gogvadze, B. Zhivotovsky, *Annu. Rev. Pharmacol. Toxicol.* **2007**, *47*, 143.

[56] S. Dwivedi, Q. Saquib, A. A. Al Khedhairy, J. Musarrat, *Toxicology* **2012**, 302, 77.

[57] G. Kanimozhi, N. R. Prasad, S. Ramachandran, K. V. Pugalendi, *Eur. J. Pharmacol.* **2011**, *672*, 20.

[58] Y. Lu, T. Pang, J. Wang, D. Xiong, L. Ma, B. Li, Q. Li, S. Wakabayashi, *Biochem. Biophys. Res. Commun.* **2008**, *377*, 441.

[59] S. S. Kannurpatti, B. G. Sanganahalli, S. Mishra, P. G. Joshi, N. B. Joshi, *Neurochem. Int.* **2004**, *44*, 361.

[60] E. C. Toescu, A. Verkhratsky, *Pflugers Arch.* **2000**, *440*, 941.

[61] P. Bernardi, V. Petronilli, F. Di Lisa, M. Forte, *Trends Biochem. Sci.* **2001**, *26*, 112.

[62] J. Levraut, H. Iwase, Z. H. Shao, T. L. V. Hoek, P. T. Schumacker, *Am. J. Physiol.: Heart Circ. Physiol.* **2003**, *284* , H549.

[63] J. Y. Lee, G. Y. Jung, H. J. Heo, M. R. Yun, J. Y. Park, S. S. Bae, K. W. Hong, W. S. Lee, C. D. Kim, *Toxicol. Lett.* **2006**, *166*, 212.

[64] R. Zhou, A. S. Yazdi, P. Menu, J. Tschopp, *Nature* **2010**, *469*, 221.

[65] J. D. Hooker, V. H. Nguyen, V. M. Taylor, D. L. Cedeño, T. D. Lash, M. A. Jones, S. M. Robledo, I. D. Vélez, *Photochem. Photobiol.* **2012**, *88*, 194.

[66] N. Lin, H. Chen, H. Zhang, X. Wan, Q. Su, *Endocrine* **2012**, *42*, 107.

초 록

광역동 치료를 위하여 광감각제인 protoporphyrin IX 와 실리카 나노구조를 기반으로 하는 효율적인 항암제를 개발하였다. 효과적인 약물전달을 위하여 약 50 nm 의 실리카/티타니아 중공구조 구형나노입자를 제조하고 내부에 광감각제를 충전시켰다. 항암제의 효과를 증진시키기 위해 나노입자 표면에 암세포에 표적지향성을 가지는 엽산을 수식하였다. 개발한 항암제의 효과를 알아보기 위해 MCF-7 세포주와 SK-BR-3 세포주를 이용하였다. MCF-7 세포는 엽산에 민감한 세포주이다. 세포에 대한 나노입자의 효과는 세포 생존 능력, 생 세포 현미경, 투과 전자 현미경, 미토콘드리아 기능이상 실험을 통해 체계적으로 조사되었다. 엽산의 표적화 효과로 인해 MCF-7 세포에서 SK-BR-3 세포 보다 높은 항암 효과가 관찰되었다. 또한 항암 효과는 나노입자 농도와 빛의 조사 시간에 비례하는 경향을 나타냈다. 반면에 엽산이 수식되지 않은 나노입자는 표적지향성을 보이지 않고 두 종류의 세포 모두에서 낮은 독성을 보였다. 이러한 연구 결과는 표적지향성을 지니는 실리카/티타니아 중공구조 구형나노입자를 이용한 광역동 치료가 항암제로써 응용 가능성을 보임을 사료한다.

주요어 : 중공 구형나노입자, 광역동치료, 약물전달, 표적지향성, 항암제.
학번 : 2012-22585